Multiscale mechanical characterization of hybrid Ti/PMMA layered materials

M. Reggente, M. Natali, D. Passeri, M. Lucci, I. Davoli, G. Pourroy, Patrick Masson, H. Palkowski, U. Hangen, A. Carradò, et al.

Multiscale mechanical characterization of hybrid Ti/PMMA layered materials

M. Reggente[a,b], M. Natali[a], D. Passeri[a,*], M. Lucci[c], I. Davoli[c], G. Pourroy[b], P. Masson[b], H. Palkowski[d], U. Hangen[e], A. Carradò[b], M. Rossi[a,f]

a Department of Basic and Applied Sciences for Engineering, SAPIENZA University of Rome, Italy
b Université de Strasbourg, Institut de Physique et Chimie des Matériaux de Strasbourg, UMR 7504 CNRS, France
c Department of Physics, University of Rome Tor Vergata, Italy
d Institute of Metallurgy, Clausthal University of Technology, Clausthal-Zellerfeld, Germany
e Bruker BNA GmbH, Dennewartstrasse 25, 52068 Aachen, Germany
f Research Center for Nanotechnology applied to Engineering of SAPIENZA University of Rome (CNIS), Italy

Keywords: Metal–polymer interface, Grafted polymers, Poly(methyl methacrylate), Atomic force microscopy (AFM), Contact resonance atomic force microscopy (CR-AFM), Multiscale mechanical techniques

Abstract:
Metal surfaces coated with organic layers are innovative materials with high potential for many industrial applications. To overcome the limitations due to the generally poor adhesion between these two components, polymers covalently anchored onto the substrate ('grafted' polymers) have been proposed as adhesives interlayers. Their mechanical properties, however, strongly affect their performances and thus have to be characterized at different scales. In this paper we report the mechanical characterization of thick poly(methyl methacrylate) (PMMA) layers grafted on titanium substrates using standard nanoindentation as well as different AFM-based techniques, namely AFM-based nanoindentation, contact resonance AFM (CR-AFM), HarmoniX™, and PeakForce quantitative nanomechanical mapping (PF-QNM™). The specific results obtained with each technique reflect the mechanical properties at different scales for these multiscale systems. Thus, these methods constitute a unique set of techniques for the complete analysis of the mechanical response of advanced materials from the macro- down to the nanoscale.

1. Introduction:

Modification of metal surface properties by coating them with organic layers is a field of extreme interest in many industrial sectors, from electronics to automotive and biomedical applications, since it allows tailoring several interfacial properties, such as adhesion, wetting, elasticity and biocompatibility [1]. Because metals and polymers do not spontaneously chemically bond, the main issue related to these metal/polymer systems concerns their weak adhesion. Additionally, residual stresses in such systems may result in premature and undesirable delimitation phenomena affecting the life-time of the entire system [2]. In order to improve their in-service durability, recently grafted polymers (namely, polymer covalently anchored onto the substrate) have been proposed as adhesives layers to be introduced between the two components [2–5]. In particular, it has been shown that by exploiting the miscibility between end-tethered polymer chains and those of a bulk [6,7] or melt polymer, the metal/polymer adhesion strength can be enhanced [2,4,5]. Depending on the brush synthesis process as well as on the substrate surface finishing, smooth or porous and rough layers with different molecular weights may be fabricated [8]. Moreover, they can be affected by altered surface mechanical properties compared to the bulk ones, because of the higher surface mobility of the polymer chains at the interface [9]. Thus, knowing the surface mechanical properties of the grafted polymers is therefore of primary importance to control the adhesive bond which strongly relies on the physical properties (such as viscoelasticity and wettability) of the brush layer [6,8].
However, the mechanical characterization of these materials using standard techniques is not trivial as they are layered materials in which compliant polymers are grown on hard substrates. They may have nonhomogeneous thickness and can exhibit porosity within the polymer layer thickness and/or at the polymer/metal interface. Indeed, different responses can be obtained performing different mechanical tests due to the material structure, which can be considered homogeneous or not, depending on the investigation length scale. In general, the properties of multilayered, nanocomposited, multiscale, and/or hierarchically structured materials may dramatically differ when macro-, meso-, micro-, or nanoscopic volumes of material are analyzed. Therefore, multiscale mechanical characterization of these classes of materials, from the macro- or mesoscale to the micro- or nanoscale, is required, which is likely to provide different, yet complementary, results at different scales [10,11]. Thanks to its capability of positioning within a nanometer resolution on the sample surface, atomic force microscopy (AFM)

has been used as a versatile platform to develop advanced hybrid mechanical characterization methods, coupled with standard quasi-static [12–14] or dynamic [15,16] methods. Moreover, different AFM-based nanomechanical techniques – either quasi-static (in which the AFM tip is used as an indenter) or dynamic (also coupled with ultrasound based methods) – have been developed taking advantage of the positioning capability, the nanometer lateral resolution, the possibility of probing the sample with ultralow loads, and the use of a feedback system to map the sample surface with a controlled applied force. These characteristics make AFM-based methods advantageous over standard methods, in particular to study soft thin films on substrates [17,18].
In this work, we report the characterization of thick poly(methyl methacrylate) (PMMA) layers grafted on titanium substrates using standard nanoindentation as well as different AFM-based techniques, namely AFM-based nanoindentation, contact resonance AFM (CRAFM), HarmoniX™, and PeakForce quantitative nanomechanical mapping (PF-QNM™), which are characterized by different penetration depths and contact radii. Besides the interest in the mechanical study of this particular class of materials, the need for multiscale mechanical characterizations is discussed.

2. Materials:

Surface initiated atom transfer radical polymerization (SI-ATRP) was used to synthesize Ti/PMMA interfaces. Briefly, bromoisobutyrateundecenyl-1-phosphonic acid ATRP initiators, synthesized as elsewhere reported [19], were immobilized on commercially pure Ti disks following the 'grafting from' method [20,21]. Then, starting from the initiator modified Ti surfaces, poly(methyl metacrilate) (PMMA) chains were grown through an ATRP technique using a transition metal complex consisting of copper(I) bromide (CuBr) complexed with the ligand N,N,N',N'',N''-pentamethyldiethylenetriamine (PMDETA). The surface morphology and the sample cross-section were investigated by scanning electron microscopy (SEM). In particular, Ti/PMMA crosssections were prepared with a cross section polisher which uses an argon ion beam to perpendicularly hit the sample surface and sputter an amount of material, uncovering its cross-section. The chemical composition of the PMMA layer was assessed by Fourier transform infrared spectroscopy (FTIR).
Accurate mechanical measurements of the Ti/PMMA sample were carried out using different reference materials to calibrate the AFM based methods. A polystyrene (PS) and low density polyethylene (LDPE) blend (PS-LDPE, Bruker), consisting of a PS matrix in which round-shaped regions of LDPE are dispersed, in form of a film on a Si substrate, was used as the calibration reference for HarmoniX™ and PFQNM ™. For the sake of accuracy of the calibration procedure, the indentation modulus of the PS-LDPE reference sample was characterized using dynamic nanoindentation. A Hysitron TI-950 was used to perform the nanoindentation experiments with a Berkovich indenter probe. The tip area function was calibrated on a fused quartz standard sample prior to the experiment. The depth profiles of hardness and reduced modulus were determined using a CMX load function (CMX =continuous measurement of X; X= hardness, modulus, etc.) in which a quasistatic force is superimposed with an oscillating force. The harmonic frequency used was 110 Hz and the displacement amplitude was around 1 nm. The PS matrix was found to have an indentation modulus (MPS) equal to 2.3 ± 0.1 GPa, while the indentation modulus of the LDPE regions (MLDPE) is about 150 MPa.
A commercial 0.5 mm thick PMMA sheet was used to calibrate AFM nanoindentation. Both the commercial PMMA and the PS-LDPE reference samples were used to calibrate CR-AFM. The indentation modulus of the PMMA sheet (MPMMA) was determined by standard nanoindentation and found equal to 4.1 ± 0.4 GPa.

3. Methods:

3.1. Nanoscale methods: atomic force microscopy based methods

3.1.1. Atomic force microscopy based nanoindentation

The working principle of AFM nanoindentation is similar to that of the common indentation technique that uses a nanoindenter as probe. Force-penetration curves are recorded and elaborated with a suitable contact-mechanics model in order to determine the Young's modulus (E) [22,23]. Compared with the nanoindenter, AFM nanoindentation is preferably employed to characterize soft materials, since it can operate with smaller force and consequently with smaller deformations [24]. In AFM-indentation, force-distance curves are acquired, which describe the evolution of the tip-sample interaction force (F) versus the displacement (Δz) of the microscope piezoelectric scanner. These curves are obtained by recording the cantilever deflection (d) as a function of Δz during the tip approaching and retrying phases. Once that d is measured, it is multiplied by cantilever spring constant (k_c) to be transformed into F. On stiff materials, which are not indented by the AFM tip, any variation of Δz results in a variation of d of the same amount. Instead, on compliant materials, the tip indents the sample

surface. Thus, for the same value of d, Δz is bigger than that observed on hard materials. The actual penetration depth h can be evaluated as h = Δz − d. Thus the force-distance curves can be transformed into the force-indentation ones by calculating h for each point of the deflection curve [22], which can be used to evaluate the mechanical properties of the sample, i.e., hardness (H) and indentation modulus (M). In particular, the latter can be determined using well established procedures borrowed from standard depth sensing indentation [25–27]. In particular, M is evaluated from the initial slope of the unloading force-indentation curve, i.e., the contact stiffness k*, the maximum applied load F_{max} and the maximum penetration depth h_{max}, once the tip curvature radius R_t is calibrated [28–31].

AFM nanoindentation measurements have been carried out by performing single point force measurements with a commercial AFM setup (Solver, NT-MDT, Russia) equipped with a commercial Si tip (NSC16, MikroMasch) on a commercial PMMA sheet and on the synthesized Ti/PMMA samples. When needed, force values were determined from cantilever deflection using the nominal value of k_c supplied by the producer. The experimental procedure was analogous to the one previously reported [32,33]. In particular, during the analysis of cantilever deflection versus displacement curves, the contact point during the approach phase was determined by visual inspection of the curves. Curves in which the initial contact point could not be univocally determined were discarded from the subsequent data processing. The tip radius was calibrated using the commercial PMMA sheet, the indentation modulus of which was previously determined as high as MPMMA = 4.1 ± 0.4 GPa using standard nanoindentation. Several force-indentation curves, recorded increasing the indentation depth from 65 nm to 150 nm, were collected on the Ti/PMMA surfaces and the corresponding values of indentation modulus ($M_{Ti/PMMA}$) were derived.

3.1.2. Contact resonance atomic force microscopy

Contrary, to AFM nanoindentation, contact resonance AFM (CRAFM) [34–36] represents a versatile tool to perform not only single point measurements of the elastic modulus, but also to obtain quantitative maps of the sample surface mechanical properties with nanometrical lateral resolution [37,38]. In this technique the sample back side is coupled to a piezoelectric transducer which makes it vibrate with ultrasonic frequencies. By analyzing the deflection signal of the cantilever when the tip is in contact with the sample surface, the contact resonance frequencies (CRFs) of the sample-tip-cantilever system are determined. They are related to the local value of sample indentation modulus (M_s), i.e., the higher M_s, the higher the value of CRF of the generic nth mode (f_n). In the CR-AFM experimental procedure, first the resonance frequencies of the cantilever oscillating in air, far away from the sample surface, are recorded in order to evaluate a characteristic parameter of the cantilever (c_c) which combines geometrical and material properties [39]. Then, the tip is brought in contact with the sample surface. The tip-sample contact is modeled as a linear spring, the elastic constant of which is the contact stiffness k*, which depends on Ms and determines the values of the CRFs. Assuming a suitable simplified model for the cantilever [40,41], k* can be expressed as a function of f_n and the actual position of the tip on the cantilever. If the tip is located at position L_1 from the cantilever clamped end, k* is expressed as $k^*(f_n, r)$ where $r = L_1/L$, being L the cantilever length. The parameter r, generally unknown, is either estimated by SEM characterization or evaluated detecting the CRFs corresponding to two different modes (namely, f_n and f_m with $n \neq m$) and matching the two corresponding contact stiffness values by numerically solving the equation $k^*(f_n, r) = k^*(f_m, r)$. In this study, this latter method was employed. Once r is estimated, the experimentally determined values of f_n are used to calculate the local contact stiffness k*. Afterward, assuming a suitable contact mechanics [42], e.g., the Hertzian theory, M_s can be evaluated after calibration of the radius R_t and the indentation modulus M_t of the tip using a set of reference materials with known mechanical properties [43,44]. In addition to elastic modulus, CR-AFM can be used to analyzed viscoelastic properties of materials, i.e., the storage and loss moduli (E′ and E″, respectively) and the loss tangent $\tan\delta = E''/E'$, by acquiring and analyzing the values of CRFs and their corresponding quality factors Q [45]. Notably, while the accurate determination of E′ and E″ requires the calibration of the tip using reference materials, sets of f_n and Q_n can be used to evaluate tanδ without calibration [46]. Thus, CR-AFM can be used to acquire accurate quantitative maps of tanδ with nanometer lateral resolution [47].

In this work, CR-AFM experiments were performed using an AFM setup (Solver, NT-MDT, Russia) equipped with a commercial Si cantilever (CSG10, NT-MDT, Russia) with nominal dimensions L = 250 μm (length), w = 35 μm (width), t= 1 μm (thickness) and nominal spring constant k_c= 0.1 N/m. The commercial PMMA sheet and the PS regions of the PS-LDPE sample were used as reference materials for calibration purposes. For each material, e.g., the Ti/PMMA investigated sample and the PS and PMMA references, the first and the second modes were analyzed by mapping f_1 and f_2, in order to have number of probed points on the sample surfaces suitable for statistics. Averaged values of f_1 and f_2 were used to calculate k*. In particular, first we acquired f_1 and f_2 maps of the PMMA sheet which was expected to be the stiffer sample; then we mapped f_1 and f_2 of the Ti/PMMA specimens and finally those of the PS reference material. In addition, PMMA sheet was further measured after the PS to ensure

the stability of the procedure and to verify the absence of drift to due the increase of the tip radius as the result of tip wear [48]. Different zones of the samples were investigated and the entire experimental cycle was repeated twice under the same conditions. Afterwards, the f_1 and f_2 maps were post-processed and their statistics were used to determine k* for all the samples and finally to evaluate $M_{Ti/PMMA}$. Finally, CR-AFM was used to carry out a preliminary study of viscoelastic properties of Ti/PMMA. For this purpose, we acquired the values of f_1 and f_2 and the corresponding quality factors Q_1 and Q_2 on both the Ti/PMMA and the commercial bulk PMMA. The values of tanδ were then calculated as detailed elsewhere [49].

3.1.3. HarmoniX™

In the HarmoniX™ mode, the sample surface is imaged in tapping mode with a T-shaped cantilever with a tip placed out of the cantilever axis [50,51]. Because of the particular geometry, tip-sample interaction forces generate a torque around the cantilever axis which excites the torsion of the cantilever. If the sample under investigation is sufficiently soft, the tip indents the surface during the lower portion of every oscillation cycle during tapping. Flexural oscillation signal is used to reconstruct the surface topography, as in a conventional AFM tapping mode. Simultaneously, the torsional signal, characterized by a higher signal-to-noise ratio compared to flexural one, is acquired, analyzed, and used to reconstruct force-distance curves at each point of the scanned area. After a proper calibration of the tip geometry and instrument sensitivity performed using a reference sample, these curves are in real-time analyzed using the Derjaguin–Muller–Toporov (DMT) model [52,53]. In the DMT model, the force acting on a flat surface indented by a spherical tip is expressed by

$$F = 4/3[E^*(R_t)^{1/2}(h)^{3/2}] + F_{adh} \qquad \text{(Eq 1)}$$

where F_{adh} is the tip-sample adhesion force and $E^* = (1/M_s+1/M_t)-1$. In case of soft materials (like polymers) indented by a stiff tip, $E^* = M_s$ can be assumed. Simultaneously to topography and phase imaging, thus, M_s, F_{max}, F_{adh}, and the energy dissipated during each cycle of tapping are mapped [18]. Force curves obtained in this study indicated that F_{adh} is about 10% of F_{max}.

In this work, nanomechanical mapping using HarmoniX™ mode was carried out with a commercial AFM system (Dimension Icon, Bruker) equipped with commercial Si T-shaped cantilevers (HMX10, Bruker). When needed, force values were determined from cantilever deflection using the nominal value of k_c supplied by the producer. HarmoniX™ experiments, calibration using the PS-LDPE reference sample, and post-experiment data processing were performed as previously detailed [54].

3.1.4. Peak force quantitative nanomechanical mapping™

Peak force quantitative nanomechanical mapping (PF-QNM™) is a recently introduced imaging mode which allows one to map the local elastic properties, tip-sample adhesion, maximum sample deformation, and energy dissipation with lateral nanometer resolution [55–57]. In peak force mode, the cantilever is made oscillate well below its resonant frequency (usually between 1 and 2 kHz), and the peak force, i.e., the maximum tip-sample force F_{max}, is used as feedback control parameter and kept constant during the scanning. During each interaction cycle, a force curve is collected and analyzed. As in HarmoniX™, after a proper tip calibration using a reference sample with well-known indentation modulus, the unloading portion of the curves are analyzed using the DMT mode and the indentation modulus is in real-time determined. Thus, maps of M_s, maximum deformation, F_{adh}, and energy dissipated during each cycle are acquired simultaneously with topographical images [55–57].

In this work, PF-QNM™ experiments were carried out with a commercial AFM system (Dimension Icon, Bruker) equipped with commercial Si tips (RTESP, Bruker), using a F_{max} value of 80 nN. When needed, force values were determined from cantilever deflection using the nominal value of kc supplied by the producer. Calibration was performed using the PS-LDPE reference sample.

3.2. Standard methods: depth sensing nanoindentation

Indentation modulus of was determined using standard depth sensing (nano)indentation (DSI, Nano Test Micro Materials Ltd.) using a diamond cone tip with an angle of 90° and a radius of 25 µm. Force-indentation curves were obtained with maximum load values of 0.2 mN, 0.4 mN, 0.6 mN, 1 mN, 3 mN, and 5 mN. For each value of maximum load, 25 force-indentation curves were acquired. The time of maximum fixed load was 10 s and the penetration time using load control was 30 s. Indentation modulus was calculated using data taken from the slope of the tangent to the unloading curve.

4. Results and discussion:

4.1. Morphology and chemical composition of Ti/PMMA

Before the mechanical characterization, morphology and chemical composition of the Ti/PMMA samples were deeply investigated. SEM micrographies (Fig. 1a) confirm that the Ti surface is completely covered by a PMMA layer characterized by a not uniform thickness. The PMMA surface shows the presence of roughly spherical agglomerates of polymer. Moreover, the cross-section of the Ti/PMMA interface (Fig. 1b) reveals a complex porous structure with voids at the polymer substrate interface. The thickness of the PMMA layer ranges from about 100 nm to 1 µm. This complex structure is assigned to the particular Ti pretreatment which leads to a porous oxide layer from which the polymer is grown. The chemical composition of the PMMA layer was finally analyzed by FTIR analysis. The FTIR spectrum (Fig. 1c) shows the peak related to the carbonyl groups stretching (C=O, at 1730 cm^{-1}) and those pertained to the α-methyl group vibrations (α-CH_3 at 1382 cm^{-1} and 747 cm^{-1}). Thus, FTIR analysis confirms that the PMMA layer was successfully grown.

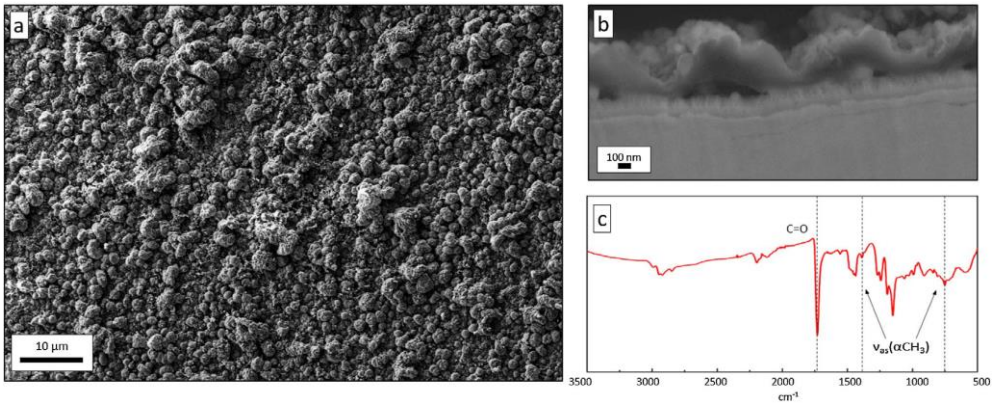

Fig. 1. (a) SEM micrograph of the Ti/PMMA samples morphology. (b) Cross-section of the Ti/PMMA interfaces highlighting the porous structure underneath the polymer layer. (c) FTIR spectrum of the grown PMMA layer.

4.2. Mechanical characterizations

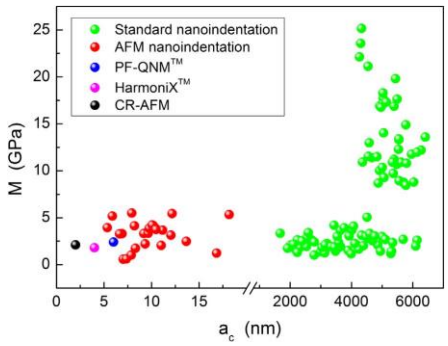

Fig. 2. Measured values of indentation modulus (M) of the Ti/PMMA sample measured using standard nanoindentation, AFM nanoindentation, CR-AFM, PF-QNM™, and HarmoniX™ as a function of the contact radius a_c.

In each of the mechanical characterizations reported in this work, the Ti/PMMA film was probed using a different tip (Berkovich indenters or AFM tips). The response of the material during mechanical tests depends on the volume of probed material, i.e., the portion of material affected by the stress field induced by the tip, which in turns depends on the tip-sample contact radius a_c [42,58]. Thus, in order to compare results of mechanical tests on layered materials obtained with different indenters, the measured indentation modulus should be plotted versus the corresponding value of a_c normalized by the film thickness [59,60]. However, in the present case, only one film is involved, the thickness of which is difficult to be determined due to the sample roughness (see the cross-section in Fig. 1b). Thus, in this work the indentation modulus values resulting from the different mechanical characterizations have been analyzed by plotting them versus the (not normalized) a_c.
Standard nanoindentation has been performed applying different values of maximum load. Thus different values of penetration depth are reached, from 70 nm to 850 nm. The obtained values of M are shown in Fig. 2 as a function of the corresponding a_c determined using the same relations used in standard nanoindentation [25–27].

At smaller contact radius, i.e., up to 4 μm, the average measured value of indentation modulus is MDSI= 2.2 ± 0.2 GPa (Table 1). At larger values of a_c, either the same values of indentation modulus or significantly larger ones are obtained depending on the actual point on the surface. The bigger values of indentation modulus can be rationalized invoking a more severe effect of the Ti substrate on DSI measurements. Therefore, the presence of dramatic variation of M in correspondence of a_c > 4μm suggests that the polymer layer thickness is not uniform. Conversely, the value M_{DSI}= 2.2 ± 0.2 GPa obtained for a_c < 4μm is significantly lower than that measured on the commercial bulk PMMA sheet (MDSI= 4.1 ± 0.4 GPa). In principle, this is not surprising as it is well known that mechanical properties of polymers may significantly vary depending on the actual synthesis procedure. Nevertheless, we think that the actual reduction of indentation modulus is ascribable to the voids at the polymer–substrate interface. Indeed, voids cause the reduction of the indentation modulus values measured with DSI [61,62] as well as with AFM-based techniques such as CR-AFM [63] or scanning near-field ultrasound holography [64]. Also, AFMbased methods, such as CR-AFM, have been demonstrated to be sensitive to delaminations and lack of adhesion at buried film-substrate interfaces [65,66]. Thus, the value of indentation modulus retrieved using DSI describes the mechanical response of the 'porous film' for a_c < 4μm and of the system constituted by the 'porous film' plus the stiff substrate for a_c > 4μm.

Technique	$M_{Ti/PMMA}$ (GPa)	a_c (nm)
Standard nanoindentation	2.2 ± 0.2	2000–4000
AFM nanoindentation	3.3 ± 0.6	5–20
PF-QNM™	2.4 ± 0.3	6
HarmoniX™	1.8 ± 0.5	4
CR-AFM	2.1 ± 0.3	2

Table 1: Average value of the indentation modulus of the Ti/PMMA sample $M_{Ti/PMMA}$ measured with the different techniques and the corresponding values of contact radius a_c.

AFM nanoindentation experiments were performed in order to obtain results from shallower indentation tests, i.e., with values of ac in the range 5–20 nm. Indentation modulus values obtained with AFM nanoindentation are shown in Fig. 2 as a function of a_c. As it is clear from Fig. 2, data obtained using AFM indentation are more scattered than those obtained by DSI. This results in a bigger relative uncertainty in the mean value of indentation modulus retrieved with AFM nanoindentation, i.e., 3.3 ± 0.6 GPa (Table 1). This is not surprising as the smaller R_t, and thus the smaller a_c, enables one to perform indentations of the sample more local than those obtained with DSI. Indeed, referring to the topography reported in Fig. 1a, the values of a_c as high as some microns, typical of DSI, imply that several agglomerates of polymer are probed during a single indentation. Thus, the sub-micron structures in Fig. 1b are not mechanically resolved. Therefore, the variations in the value of M measured with DSI, reflecting the more or less significant effect of the substrate, are due to variations in the average value of the film thickness. On the contrary, the values of a_c in AFM nanoindentation enable one to resolve the local variations in film thickness observable in Fig. 1b. In other words, AFM nanoindentation could be affected (even if partially) by the effect of the substrate mechanical properties in correspondence of the valleys between two adjacent agglomerates where the thickness is smaller [67]. Conversely, it could probe the mechanical response of the PMMA film unaffected by the presence of voids in correspondence of the peaks of the agglomerates. In the latter case, the measured value of M is compatible within the experimental uncertainty with the indentation modulus of bulk PMMA measured with DSI.

AFM-based techniques have the unique advantage over standard nanoindentation that can be used to carry out nanomechanical mapping with lateral resolution comparable with the dimension of the AFM tip. For example, AFM nanoindentation has been used to realize mechanical tomography at the nanoscale [68,69]. In this work, CR-AFM, PF-QNM™, and HarmoniX™ experiments have been performed in order to probe and map the elastic modulus of the surface of the Ti/PMMA sample with higher lateral resolution. The statistics of the values of the first CRF measured on the Ti/PMMA and the two references (PMMA and PS) are shown in Fig. 3a. The values of f_1 of Ti/PMMA are lower than those of the two references, indicating that these latter are stiffer than the investigated sample. Moreover, the relative standard deviation of the Gaussian distribution is bigger for the Ti/PMMA than for the references.

This is partially attributable to topography-induced artifacts due to the local inclination of the surface [44] and to the modulation of the contact area in presence of grains and agglomerates [70]. Besides, the more dispersed values of CRF can be related to the mechanical properties of the Ti/PMMA sample less homogeneous than those of the two reference materials due to the presence of subsurface voids and the substrate-film interface. It has been demonstrated, indeed, that although CR-AFM is a 'surface' characterization technique, it is sensitive to

buried mechanically nonhomogeneous features (like voids or stiff nanoparticles in polymer-based nanocomposites) typically located a few hundreds of nanometers below the surface [63,71]. The modulation of the indentation modulus on the Ti/PMMA surface is evident from CR-AFM nanomechanical mapping. As an example, Fig. 3b and c show the topography of an area of the Ti/PMMA sample and the corresponding indentation modulus map, respectively. From statistics on the indentation modulus maps, the indentation modulus retrieved with CRAFM can be evaluated as M_{CR-AFM}= 2.1 ± 0.3 GPa and the corresponding value of a_c calculated using the Sneddon approach [25,26] is 2 nm (Table 1). Although the value of M_{CR-AFM} compatible with that obtained with AFM nanoindentation, the contact radius suggests that CR-AFM is not sensitive to the presence of buried voids which, therefore, cannot be invoked to justify the value of M_{CR-AFM} lower than that obtained with AFM indentation. The reduction of the modulus can be attributable to the effect of the very first layers of polymer, which have been reported to be softer with respect of the bulk [72–75].

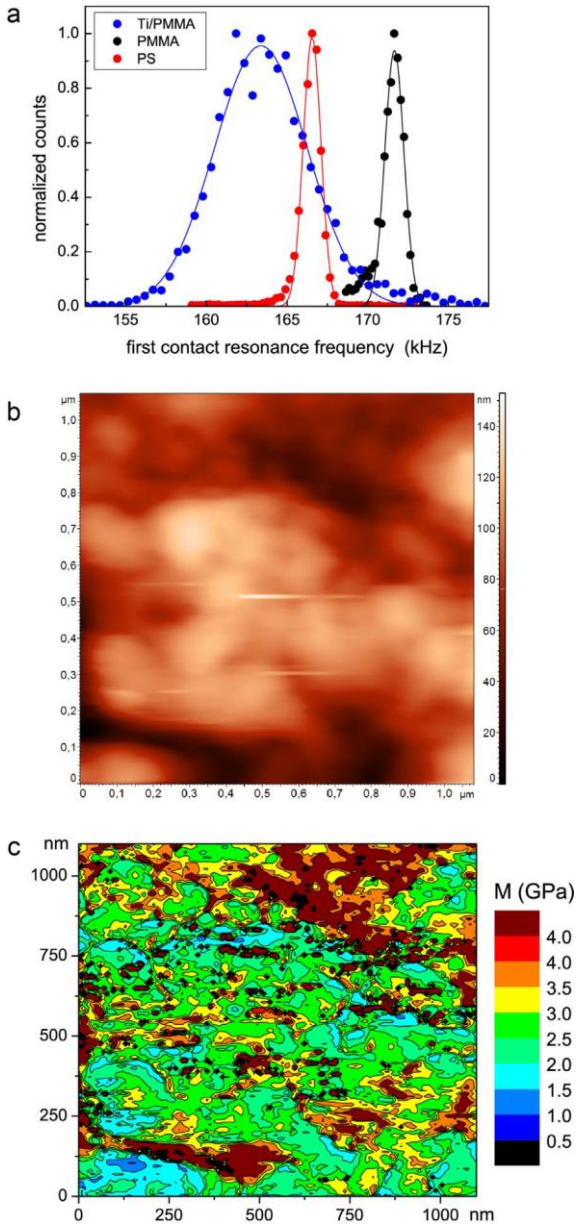

Fig. 3. Example of CR-AFM nanomechanical characterization. (a) Histograms (symbols) and corresponding Gaussian fit (solid lines) of the values of the first CRF measured on the Ti/PMMA and on the two reference materials (PMMA and PS). (b) Topography and (c) map of the indentation modulus map reconstructed from the first and the second CRFs images acquired on the surface of the Ti/PMMA sample.

Shallow indentations were attained also using HarmoniX™. An example of topography and corresponding indentation modulus map retrieved with this technique is shown in Fig. 4a and b, respectively. From the latter, the indentation modulus values of 1.8 ± 0.5 GPa is obtained (Table 1). Clearly distinguishable topography-induced

mechanical artifacts are responsible for the apparent modulation of the indentation modulus measured on the Ti/PMMA. Statistics on the modulus maps (Fig. 4c) indicate that the distribution corresponding to the Ti/PMMA sample is broader than that corresponding to the PS reference. We attribute this result to the sole effect of modulation of the tip-sample contact area. Indeed, although HarmoniX™ has been reported to be sensitive to subsurface variation of elastic modulus in case of ultra-thin samples [76], in the present case even the thinnest areas of the PMMA layer are too big compared to the contact radius (calculated as small as 4 nm determined using the DMT model, i.e., Eq. (1)) to allow one to detect buried voids or the substrate–film interface. Again, the reduction ascribable to the effect of the very first layers of polymer invoked discussing CR-AFM results can be considered also in this case to rationalize the value of M lower than the bulk one.

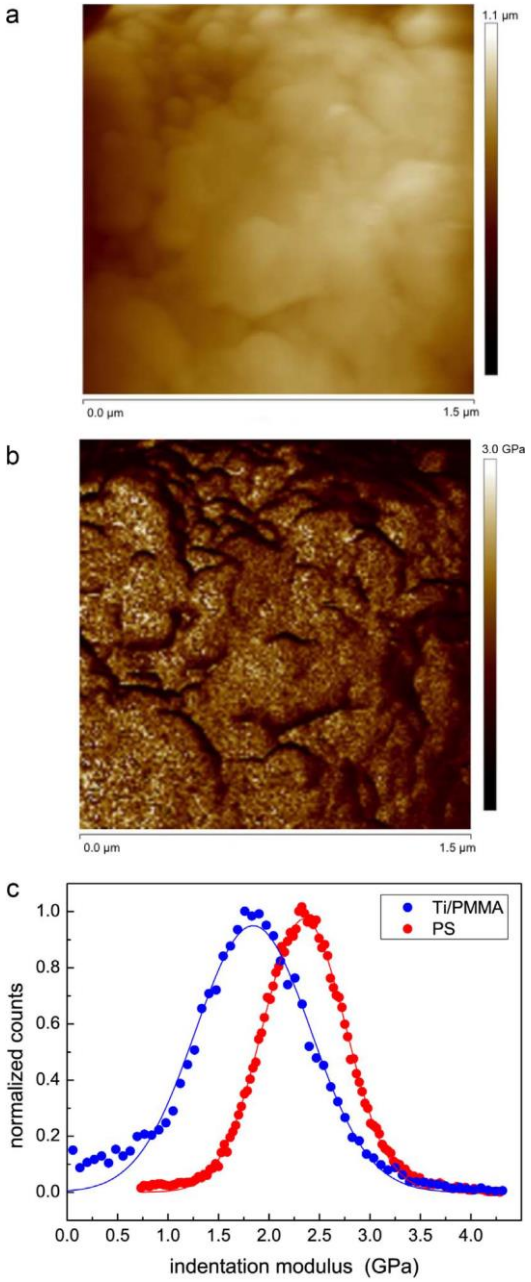

Fig. 4. Example of HarmoniX™ nanomechanical characterization. Topography (a) and indentation modulus map (b) of the Ti/PMMA surface. (c) Histograms of the indentation modulus values (symbols) and corresponding Gaussian fit (solid lines) obtained on Ti/PMMA and PS

PF-QNM™ results confirm those obtained using CR-AFM and HarmoniX™. An example of topography and corresponding indentation modulus map retrieved with this technique is shown in Fig. 5a and b, respectively, while statistics of the measured indentation modulus are reported in Fig. 5c. The measured indentation modulus 2.4 ± 0.3 GPa (Table 1) is compatible with the values retrieved with CR-AFM and HarmoniX™. Also, the tip-sample

contact radius is estimated as small as 6 nm using the DMT model, i.e., Eq. (1), which is similar to the value obtained with the other two techniques. Also in this case, the lower indentation modulus can be caused by the presence of a softer layer of polymer on the sample surface.

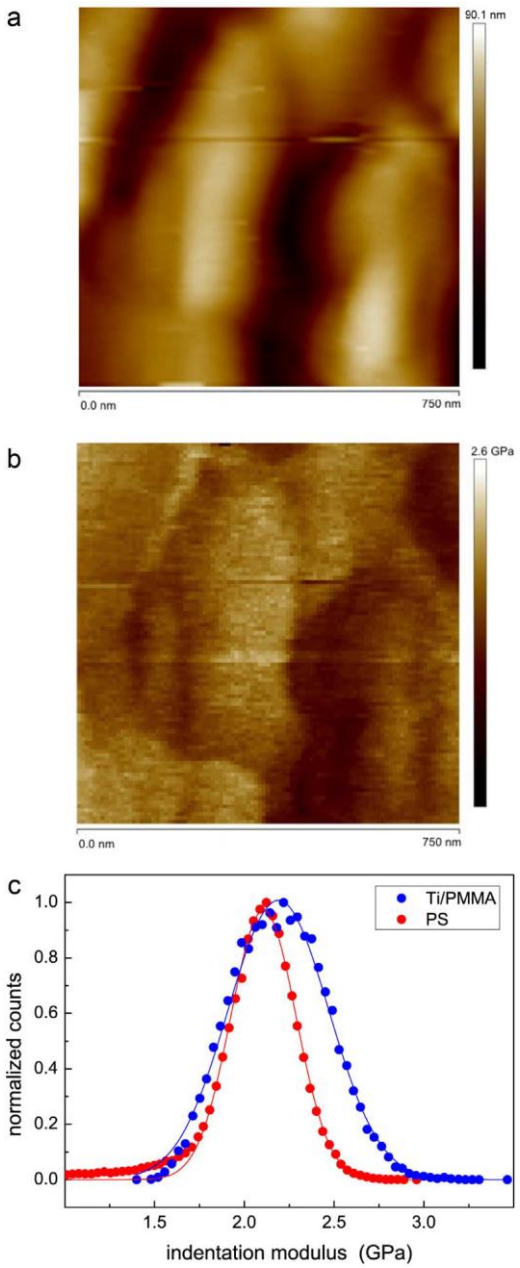

Fig. 5. Example of PF-QNM™ nanomechanical characterization. Topography (a) and indentation modulus map (b) of the Ti/PMMA surface. (c) Histograms of the indentation modulus values (symbols) and corresponding Gaussian fit (solid lines) obtained on Ti/PMMA and PS.

Except for the measurements with standard DSI at larger contact radius which are obviously affected by the substrate properties, the comparison of the results obtained using the different techniques clearly shows compatible results. The smaller contact radii of AFM techniques enable one to perform local mechanical measurements which, therefore, are more sensitive to the local conditions of the sample (local thickness, homogeneity) and are more affected by topography-induced artifacts. In addition, due to the different contact radii, the different techniques reflect different mechanical properties of the system. Indeed, standard nanoindentation probes the whole system formed by the PMMA matrix and the subsurface voids. Conversely, AFM nanoindentation data are more scattered as the technique locally probes the sample surface and the average indentation modulus reflects more the properties of the bulk PMMA matrix without being affected by the subsurface voids. Dynamic AFM methods like CR-AFM, PF-QNM™, and HarmoniX™, conversely, are more affected by the very superficial

nanomechanical properties of the investigated sample and, thus, are the most suitable to study the effect of surface treatments of polymers.
Finally, it is worth mentioning that AFM-based methods can be used to map other mechanical parameters besides indentation modulus which may be of interest for the applications of polymer-metal layered materials. For example, PF-QNM™ and HarmoniX™ allow one to collect maps of tip sample adhesion forces. Preliminary characterization of the adhesion using PF-QNM™ with the same AFM tip seems to indicate that the tip-sample adhesion on the Ti/PMMA is about 140% of that on the commercial PMMA, which may indicate differences in the adhesion and/or in the hydrophobicity/hydrophilicity. Also, we assessed viscoelastic properties of the Ti/PMMA sample using CR-AFM for viscoelasticity, i.e., we acquired the values of the first and second CRFs and the corresponding Q factors to evaluate tanδ. We measured tanδ = 0.024 for the commercial bulk PMMA, which is in good agreement with results obtained in the same range of frequencies and reported in literature [77]. Conversely, we calculated tanδ =0.043 for the Ti/PMMA sample, indicating a material with a more viscoelastic mechanical response with respect to the commercial PMMA, which shows a more elastic response.
Although these results requires more detailed studies, adhesion mapping using PF-QNM™ or HarmoniX™ and viscoelastic mapping using CR-AFM may represent a useful tool for the characterization of nanoscale properties of polymer-metal layered materials to be related to mesoscopic and macroscopic properties.

5. Conclusions:

In conclusion, we reported a study on the mechanical properties of thick PMMA layers grafted on Ti substrates using standard nanoindentation as well as different AFM-based techniques. The combined approach resulting from the synergistic use of the different methods allowed us to investigate the sample mechanical properties varying the tip-sample contact radius from a few nanometers to ten microns. Depending on the contact radius, each technique enabled us to investigate specific aspects of the mechanical response of these materials, which represent complex systems formed by a 'porous' polymeric film on a stiff metal substrate. Besides the interest in the specific properties of the grafted PMMA, this study highlights how the characterization of multiscale, nanocomposited, hierarchically structured materials requires the combined use of different methods sensitive to different volumes of material. These methods constitute a multiscale set of techniques which is strictly needed for a complete analysis of the mechanical response of advanced materials from the macro- down to the nanoscale.

Acknowledgements:

The authors acknowledge useful discussions with J.J. Vlassak about indentation of porous materials and J. Faerber and L. Loos for SEM analysis and cross-section preparation. This work has benefitted from the financial support of the MICA Carnot Institute and the 'NANOTRANSMED' project co-funded by the European Regional Development Fund (ERDF) in the framework of the INTERREG V Upper Rhine program 'Transcending borders with every project'.

References:

[1] L. Wu, J. Baghdachi, Functional Polymer Coatings: Principles, Methods, and Applications vol. 12, John Wiley & Sons, 2015.
[2] C. Sun, F. Zhou, L. Shi, B. Yu, P. Gao, J. Zhang, W. Liu, Tribological properties of chemically bonded polyimide films on silicon with polyglycidyl methacrylate brush as adhesive layer, Appl. Surf. Sci. 253 (4) (2006) 1729–1735.
[3] Y. Shaulov, R. Okner, Y. Levi, N. Tal, V. Gutkin, D. Mandler, A.J. Domb, Poly(methyl methacrylate) grafting onto stainless steel surfaces: application to drugeluting stents, ACS Appl. Mater. Interface 1 (11) (2009) 2519–2528.
[4] K. Shimizu, K. Malmos, A.H. Holm, S.U. Pedersen, K. Daasbjerg, M. Hinge, Improved adhesion between PMMA and stainless steel modified with PMMA brushes, ACS Appl. Mater. Interface 6 (23) (2014) 21308–21315.
[5] O. Alageel, M.-N. Abdallah, Z.Y. Luo, J. Del-Rio-Highsmith, M. Cerruti, F. Tamimi, Bonding metals to poly(methyl methacrylate) using aryldiazonium salts, Dent. Mater. 31 (2) (2015) 105–114.
[6] W.V.S. Gutowski, Interface/interphase engineering of polymers for adhesion enhancement: Part I. Review of micromechanical aspects of polymer interface reinforcement through surface grafted molecular brushes, J. Adhes. 79 (5) (2003) 445–482.
[7] S.W. Sides, G.S. Grest, M.J. Stevens, S.J. Plimpton, Effect of end-tethered polymers on surface adhesion of glassy polymers, J. Polym. Sci. Polym. Phys. 42 (2) (2004) 199–208.
[8] D. Julthongpiput, M. LeMieux, V.V. Tsukruk, Micromechanical properties of glassy and rubbery polymer brush layers as probed by atomic force microscopy, Polymer 44 (16) (2003) 4557–4562.

[9] B. Zhao, W.J. Brittain, Polymer brushes: surface-immobilized macromolecules, Prog. Polym. Sci. 25 (5) (2000) 677–710.
[10] P. Schön, S. Dutta, M. Shirazi, J. Noordermeer, G.J. Vancso, Quantitative mapping of surface elastic moduli in silica-reinforced rubbers and rubber blends across the length scales by AFM, J. Mater. Sci. 46 (2011) 3507–3516.
[11] K. Sweers, K. van der Werf, M. Bennink, V. Subramaniam, Nanomechanical properties of α-synuclein amyloid fibrils: a comparative study by nanoindentation, harmonic force microscopy, and Peakforce QNM, Nanoscale Res. Lett. 6 (2011) 270.
[12] B. Bhushan, V.N. Koinkar, Nanoindentation hardness measurements using atomic force microscopy, Appl. Phys. Lett. 64 (1994) 1653–1655.
[13] A.V. Kulkarni, B. Bhushan, Nanoscale mechanical property measurements using modified atomic force microscopy, Thin Solid Films 290 (1996) 206–210.
[14] B. Bhushan, V.N. Koinkar, Evaluation of mechanical properties in nanometer scale using AFM-based nanoindentation tester, Nanostruct. Mater. 12 (1999) 1049–1052.
[15] S.A. Syed Asif, K.J. Wahl, R.J. Colton, Nanoindentation and contact stiffness measurement using force modulation with a capacitive load–displacement transducer, Rev. Sci. Instrum. 70 (1999) 2408–2413.
[16] S.A. Syed Asif, K.J. Wahl, R.J. Colton, O.L. Warren, Quantitative imaging of nanoscale mechanical properties using hybrid nanoindentation and force modulation, J. Appl. Phys. 90 (2001) 1192–1200.
[17] D. Passeri, A. Bettucci, M. Rossi, Acoustic and atomic force microscopy for the mechanical characterization of thin films, Anal. Bioanal. Chem. 396 (2010) 2769–2783.
[18] D. Passeri, M. Rossi, E. Tamburri, M.L. Terranova, Mechanical characterization of polymeric thin films by atomic force microscopy based techniques, Anal. Bioanal. Chem. 405 (2013) 1463–1478.
[19] V. Vergnat, Matériaux hybrides organiques-inorganiques par greffage covalent de polymères sur des oxydes métalliques (Ph.D. thesis), University of Strasbourg, 2011.
[20] G. Guerrero, P.H. Mutin, A. Vioux, Anchoring of phosphonate and phosphinate coupling molecules on titania particles, Chem. Mater. 13 (11) (2001) 4367–4373.
[21] V. Vergnat, T. Roland, Effect of covalent grafting on mechanical properties of TiO_2/polystyrene composites, Mater. Chem. Phys. 147 (1–2) (2014) 261–267.
[22] A.L. Weisenhorn, M. Khorsandi, S. Kasas, V. Gotzos, H.J. Butt, Deformation and height anomaly of soft surfaces studied with an AFM, Nanotechnology 4 (1993) 106–113.
[23] J. Domke, M. Radmacher, Measuring the elastic properties of thin polymer films with the atomic force microscope, Langmuir 14 (1998) 3320–3325.
[24] H.J. Butt, B. Cappella, M. Kappl, Force measurements with the atomic force microscope: technique, interpretation and applications, Surf. Sci. Rep. 59 (2005)1–152.
[25] I.N. Sneddon, The relation between load and penetration in the axisymmetric Boussinesq problem for a punch of arbitrary profile, Int. J. Eng. Sci. 3 (1965) 47–57.
[26] G.M. Pharr, W.C. Oliver, F.R. Brotzen, On the generality of the relationship among contact stiffness, contact area, and elastic modulus during indentation, J. Mater. Res. 7 (1992) 613–617.
[27] W.C. Oliver, G.M. Pharr, Measurement of hardness and elastic modulus by instrumented indentation: advances in understanding and refinements to methodology, J. Mater. Res. 19 (2004) 3–20.
[28] E. Tomasetti, R. Legras, B. Nysten, Quantitative approach towards the measurement of polypropylene/(ethylene-propylene) copolymer blends surface elastic properties by AFM, Nanotechnology 9 (1998) 305–315.
[29] C. Reynaud, F. Sommer, C. Quet, N. El Buonia, D. Tran Minh, Quantitative determination of Young's modulus on a biphase polymer system using atomic force microscopy, Surf. Interface Anal. 30 (2000) 185–189.
[30] C.A. Clifford, M.P. Seah, Quantification issues in the identification of nanoscale regions of homopolymers using modulus measurement via AFM nanoindentation, Appl. Surf. Sci. 252 (2005) 1915–1933.
[31] D. Passeri, A. Bettucci, A. Biagioni, M. Rossi, A. Alippi, E. Tamburri, M. Lucci, I. Davoli, S. Berezina, Indentation modulus and hardness of viscoelastic thin films by atomic force microscopy: a case study, Ultramicroscopy 109 (2009) 1417–1427.
[32] D. Passeri, A. Bettucci, A. Biagioni, M. Rossi, A. Alippi, M. Lucci, I. Davoli, S. Berezina, Quantitative measurement of indentation hardness and modulus of compliant materials by atomic force microscopy, Rev. Sci. Instrum. 79 (2008) 066105.
[33] E. Tamburri, V. Guglielmotti, R. Matassa, S. Orlanducci, S. Gay, G. Reina, M.L. Terranova, D. Passeri, M. Rossi, Detonation nanodiamonds tailor the structural order of PEDOT chains in conductive coating layers of hybrid nanoparticles, J. Mater. Chem. C 2 (2014) 3703–3716.
[34] U. Rabe, W. Arnold, Acoustic microscopy by atomic force microscopy, Appl. Phys. Lett. 64 (1994) 1493–1495.

[35] U. Rabe, J. Janser, W. Arnold, Vibration of free and surface-coupled atomic force microscope cantilevers: theory and experiment, Rev. Sci. Instrum. 67 (1996) 3281–3293.
[36] U. Rabe, V. Scherer, S. Hirsekorn, W. Arnold, Nanomechanical surface characterization by atomic force acoustic microscopy, J. Vac. Sci. Technol. B 15 (1997) 1506–1511.
[37] D.C. Hurley, M. Kopycinska-Müller, A.B. Kos, R.H. Geiss, Nanoscale elastic-property measurements and mapping using atomic force acoustic microscopy methods, Meas. Sci. Technol. 16 (2005) 2167–2172.
[38] D. Passeri, A. Bettucci, M. Germano, M. Rossi, A. Alippi, A. Fiori, E. Tamburri, M.L. Terranova, J.J. Vlassak, Local indentation modulus characterization via two contact resonance frequencies atomic force acoustic microscopy, Microelectr. Eng. 84 (2007) 490–494.
[39] E. Kester, U. Rabe, L. Presmanes, P. Tailhades, W. Arnold, Measurement of Young's modulus of nanocrystalline ferrites with spinel structures by atomic force acoustic microscopy, J. Phys. Chem. Solids 61 (2000) 1275–1284.
[40] U. Rabe, Atomic force acoustic microscopy, in: B. Bhushan, H. Fuchs (Eds.), Applied Scanning Probe Methods II, 2006, pp. 37–90.
[41] U. Rabe, M. Kopycinska-Müller, S. Hirsekorn, Atomic force acoustic microscopy, in: F. Marinello, D. Passeri, E. Savio (Eds.), Acoustic Scanning Probe Microscopy, Springer-Verlag, Berlin, Heidelberg, 2012, pp. 123–153 (Chapter 5).
[42] K.L. Johnson, Contact Mechanics, Cambridge University Press, Cambridge, United Kingdom, 2003.
[43] G. Stan, W. Price, Quantitative measurements of indentation moduli by atomic force acoustic microscopy using a dual reference method, Rev. Sci. Instrum. 77 (2006) 103707.
[44] D. Passeri, M. Rossi, J.J. Vlassak, On the tip calibration for accurate modulus measurement by contact resonance atomic force microscopy, Ultramicroscopy 128 (2013) 32–41.
[45] P.A. Yuya, D.C. Hurley, J.A. Turner, Relationship between Q-factor and sample damping for contact resonance atomic force microscope measurement of viscoelastic properties, J. Appl. Phys. 109 (2011) 113528.
[46] D.C. Hurley, S.E. Campbell, J.P. Killgore, L.M. Cox, Y. Ding, Measurement of viscoelastic loss tangent with contact resonance modes of atomic force microscopy, Macromolecules 46 (2013) 9396–9402.
[47] A.B. Churnside, R.C. Tung, J.P. Killgore, Quantitative contact resonance force microscopy for viscoelastic measurement of soft materials at the solid–liquid interface, Langmuir 31 (2015) 11143–11149.
[48] S. Amelio, A.V. Goldade, U. Rabe, V. Scherer, B. Bhushan, W. Arnold, Measurement of elastic properties of ultra-thin diamond-like carbon coatings using atomic force acoustic microscopy, Thin Solid Films 392 (2001) 75–84.
[49] M. Natali, D. Passeri, M. Reggente, E. Tamburri, M.L. Terranova, M. Rossi, Contact resonance atomic force microscopy for viscoelastic characterization of polymerbased nanocomposites at variable temperature, AIP Conf. Proc. 1749 (2016) 020008.
[50] O. Sahin, S. Magonov, C. Su, C.F. Quate, O. Solgaard, An atomic force microscope tip designed to measure time-varying nanomechanical forces, Nat. Nanotechnol. 2 (2007) 507–514.
[51] O. Sahin, N. Erina, High-resolution and large dynamic range nanomechanical mapping in tapping-mode atomic force microscopy, Nanotechnology 19 (2008) 445717.
[52] B.V. Derjaguin, V.M. Muller, Y.P. Toporov, Effect of contact deformation on the adhesion of particles, J. Colloid Interface Sci. 53 (1975) 314–326.
[53] M.E. Dokukin, I. Sokolov, Quantitative mapping of the elastic modulus of soft materials with HarmoniX and PeakForce QNM AFM modes, Langmuir 28 (2012) 16060–16071.
[54] D. Passeri, A. Biagioni, M. Rossi, E. Tamburri, M.L. Terranova, Characterization of polyaniline-detonation nanodiamond nanocomposite fibers by atomic force microscopy based techniques, Eur. Polym. J. 49 (2013) 991–998.
[55] J. Adamcik, A. Berquand, R. Mezzenga, Single-step direct measurement of amyloid fibrils stiffness by peak force quantitative nanomechanical atomic force microscopy, Appl. Phys. Lett. 98 (2011) 193701.
[56] G. Pletikapic, A. Berquand, T. Misic Radic, V. Svetlicic, Quantitative nanomechanical mapping of marine diatom in seawater using peak force tapping atomic force microscopy, J. Phycol. 48 (2012) 174–185.
[57] T.J. Young, M.A. Monclus, T.L. Burnett, W.R. Broughton, S.L. Ogin, P.A. Smith, The use of the PeakForceTM quantitative nanomechanical mapping AFM-based method for high-resolution Young's modulus measurement of polymers, Meas. Sci. Technol. 22 (2011) 125703.
[58] M. Kopycinska-Müller, R.H. Geiss, J. Müller, D.C. Hurley, Elastic-property measurements of ultrathin films using atomic force acoustic microscopy, Nanotechnology 16 (2005) 703–709.
[59] H. Li, N.X. Randall, J.J. Vlassak, New methods of analyzing indentation experiments on very thin films, J. Mater. Res. 25 (4) (2010) 728–734.

[60] H. Li, J.J. Vlassak, Determining the elastic modulus and hardness of an ultra-thin film on a substrate using nanoindentation, J. Mater. Res. 24 (3) (2009) 1114–1126.
[61] Y. Xiang, X. Chen, T.Y. Tsui, J.-I. Jang, J.J. Vlassak, Mechanical properties of porous and fully dense low-κ dielectric thin films measured by means of nanoindentation and the plane-strain bulge test technique, J. Mater. Res. 21 (2) (2006) 386–395.
[62] X. Chen, Y. Xiang, J.J. Vlassak, Novel technique for measuring the mechanical properties of porous materials by nanoindentation, J. Mater. Res. 21 (3) (2006) 715–724.
[63] Z. Parlak, F.L. Degertekin, Contact stiffness of finite size subsurface defects for atomic force microscopy: three-dimensional finite element modeling and experimental verification, J. Appl. Phys. 103 (2008) 114910.
[64] G. Shekhawat, S. Avasthy, A. Srivastava, S.-H. Tark, V. Dravid, Probing buried defects in extreme ultraviolet multilayer blanks using ultrasound holography, IEEE Trans. Nanotechnol. 9 (2010) 501–505.
[65] A.F. Sarioglu, A. Atalar, F.L. Degertekin, Modeling the effect of substrate interface defects on contact stiffness for ultrasonic atomic force microscopy, Appl. Phys. Lett. 84 (2004) 5368–5370.
[66] D.C. Hurley, M. Kopycinska-Müller, E.D. Langlois, N. Barbosa III, Mapping substrate/film adhesion with contact-resonance-frequency atomic force microscopy, Appl. Phys. Lett. 89 (2006) 021911.
[67] D. Passeri, A. Alippi, A. Bettucci, M. Rossi, A. Alippi, E. Tamburri, M.L. Terranova, Indentation modulus and hardness of polyaniline thin films by atomic force microscopy, Synth. Met. 161 (2011) 7–12.
[68] C. Roduit, S. Sekatski, G. Dietler, S. Catsicas, F. Lafont, S. Kasas, Stiffness tomography by atomic force microscopy, Biophys. J. 97 (2009) 674–677.
[69] C. Roduit, G. Longo, I. Benmessaoud, A. Volterra, B. Saha, G. Dietler, S. Kasas,Stiffness tomography exploration of living and fixed macrophages, J. Mol. Recognit. 25 (2012) 241–246.
[70] G. Stan, R.F. Cook, Mapping the elastic properties of granular Au films by contact resonance atomic force microscopy, Nanotechnology 19 (2008) 235701.
[71] J.P. Killgore, J.Y. Kelly, C.M. Stafford, M.J. Fasolka, D.C. Hurley, Quantitative subsurface contact resonance force microscopy of model polymer nanocomposites, Nanotechnology 22 (17) (2011) 175706.
[72] K.F. Mansfield, D.N. Theodorou, Molecular dynamics simulation of a glassy polymer surface, Macromolecules 24 (23) (1991) 6283–6294.
[73] A.V. Zaitseva, V.M. Rudoy, O.V. Dement'eva, M.E. Kartseva, Study of polystyrene surface local mechanical properties by the atomic force microscopy, Mater. Sci. 20 (3) (2002) 37–43.
[74] J.M. Torres, C.M. Stafford, B.D. Vogt, Elastic modulus of amorphous polymer thin films: relationship to the glass transition temperature, ACS Nano 3 (9) (2009) 2677–2685.
[75] J.M. Torres, C.M. Stafford, B.D. Vogt, Manipulation of the elastic modulus of polymers at the nanoscale: influence of UV-ozone cross-linking and plasticizer, ACSNano 4 (9) (2010) 5357–5365.
[76] D. Passeri, E. Tamburri, M.L. Terranova, M. Rossi, Polyaniline-nanodiamond fibers resulting from the self-assembly of nano-fibrils: a nanomechanical study, Nanoscale 7 (2015) 14358–14367.
[77] J. Capodagli, R. Lakes, Isothermal viscoelastic properties of PMMA and LDPE over 11 decades of frequency and time: a test of time-temperature superposition, Rheol. Acta 47 (7) (2008) 777–786.